PHYSICAL REVIEW D VOLUME 40, NUMBER 8 15 OCTOBER 1989

Evolution of bubbles in a vacuum

Antonio Aurilia
Stanford Linear Accelerator Center, Stanford University, Stanford, California 94309
and Department of Physics, California State Polytechnic University, Pomona, California 91768

Marc Palmer
DATATAPE Inc., 360 Sierra Madre Villa, Pasadena, California 91109-7014

Euro Spallucci
Istituto di Fisica Teorica, Università di Trieste, Istituto Nazionale di Fisica Nucleare, Sezione di Trieste, 34100 Trieste, Italy

(Received 26 September 1988; revised manuscript received 22 May 1989)

This paper examines the evolution of spherical bubbles in a vacuum for all possible values of the controlling parameters within the context of the general-relativistic thin-wall approximation. We propose a general classification of the admissible solutions and a graphical-numerical algorithm for their explicit construction from any given set of initial data. The different sectors in the space of the parameters are identified and a map of regions is constructed where single families of solutions can exist.

I. INTRODUCTION

The dynamics of relativistic bubbles has been investigated by many authors with different applications in mind.[1–13] The evolution of bubbles in the Minkowski vacuum was analyzed long ago in Refs. 2–4 in connection with the bag model of hadrons and a classification of the admissible solutions of the bubble equation of motion was obtained.[3] In that approach, gravitational effects on the evolution of bubbles in a vacuum were considered later in Ref. 10 within the thin-wall approximation and under the assumption of spherical symmetry, thus restricting the geometry to be of the Schwarzschild–de Sitter type. Remarkably, it was found that the mechanism that generates the vacuum pressure in the bag model of strong interactions can also trigger the mechanism of vacuum decay envisaged in the inflationary scenario of the early Universe. The bubble equation of motion can be derived either from Israel's junction conditions,[13] or from an action functional modeled on the Einstein-Maxwell system[10,11,14] in general relativity. A remarkable feature of the action functional formulation is that the interior and exterior cosmological constants are introduced in a natural way through the solutions of the coupled field equations;[10] moreover, the dynamics encoded in the action functional selects positive or at most vanishing cosmological constants and excludes negative values.[10] This is not the case when bubble dynamics is discussed in the framework of a scalar field theory. In the approach based on general relativity, the potential complexities of vacuum decay associated with the spontaneous symmetry breaking of the underlying grand-unified theory are reduced, in the thin-wall approximation, to the specification of just three effective parameters: the surface tension ρ, assumed *a priori* to be positive, and the interior and the exterior vacuum energy densities Λ_- and Λ_+. In this overall picture of bubble dynamics, the missing link which has eluded us so far is a well-defined algorithm to construct the solutions of the equation of motion of the bubble for *arbitrary* values of the above parameters. The objective of this paper is to fill this gap by extending the algorithm of Ref. 3 along the lines proposed by Blau, Guendelman, and Guth[12] (BGG) for the special case of a bubble of false vacuum in the de Sitter phase separated from an infinite region of true vacuum with vanishing energy density.

To our mind, the extension of the BGG method is not only useful but necessary. Indeed, the discussion of the special solutions of bubble dynamics that we have found in the literature is somewhat fragmentary and sometimes controversial; the only papers that we are aware of where an attempt is made at a systematic classification of the solutions are those of Refs. 3, 9, and 12. The BGG paper has the virtue that, given their choice of parameters, it offers a simple and rather systematic catalog of the possible solutions. However, the admissible solutions of the equation of motion can be classified in a large parameter space and, depending on the specific values of the parameters, the solutions can play a role in different physical situations ranging from particle physics[1–4,8] to various aspects of the large-scale structure of the Universe at the present epoch.[6,8,15]

Against this background, it seems desirable to have an algorithm capable of determining all possible types of solutions together with the region in parameter space where single families of solutions can exist. Thus, in Sec. II we develop the analogy of the bubble motion with that of a particle in a potential.[10,11] Then, following the format of the BGG paper,[12] we reduce the bubble equation of motion to a dimensionless form which lends itself to a straightforward graphical and numerical analysis. In Sec. III we derive all the necessary formulas in our algorithm and discuss some definite examples.

 ©1989 The American Physical Society

II. THE EQUATION OF MOTION

In Israel's approach to bubble dynamics,[13] let Σ represent the timelike three-dimensional world track of the bubble which separates the spacetime manifold M into two distinct four-dimensional manifolds M^- and M^+, each containing Σ as its boundary. In this approach, the key ingredient in deriving the radial equation of motion of the bubble stems from the following continuity condition as one approaches Σ from M^- or from M^+. Let

$$ds_{\pm}^2 = g_{\alpha\beta}^{\pm} dx_{\pm}^{\alpha} dx_{\pm}^{\beta}$$

represent the metrics in $M^{\pm}$, so that when approaching Σ in M^+ or M^- one has to demand that

$$(ds_+^2)_\Sigma = (ds_-^2)_\Sigma = ds_\Sigma^2 ,$$

where

$$ds_\Sigma^2 \equiv g_{ij} dl^i dl^j = -d\tau^2 + R^2(\tau)(d\theta^2 + \sin^2\theta\, d\phi^2)$$

represents the intrinsic metric on Σ. Alternatively, bubble dynamics can be formulated as a gauge theory.[11] In this case the equation of motion of the bubble radius can be derived from an action functional describing the interaction between the bubble and the cosmological gauge field A, a differential three-form $A = \frac{1}{3} A_{\mu\nu\lambda} dx^\mu \wedge dx^\nu \wedge dx^\lambda$ with field strength $F = dA$ invariant under the gauge transformation $A \to A + d\Lambda$. The details of this formulation and its underlying physical basis are fully explained in Ref. 11 and will not be repeated here. The outcome of either approach is this: under the assumption of spherical symmetry, we can assign the de Sitter (or anti-de Sitter) metric with cosmological constant Λ_- to M^- and the Schwarzschild-de Sitter (or Schwarzschild-anti-de Sitter) metric with cosmological constant Λ_+ to M^+. Here, the "anti" prefix refers to the case of negative cosmological constants. If one further prescribes the value of the surface tension ρ on the bubble, then by the mechanism of the junction conditions or by the usual variational techniques in the action functional formulation, one is led to the equation of motion of the bubble radius which, in geometrical units, takes the form[7,10-12,14]

$$\left[\frac{dR}{d\tau}\right]^2 = BR^2 - 1 - \frac{E}{R}\left[\frac{\Lambda_- - \Lambda_+}{3k^2} - 1\right] + \frac{E^2}{k^2 R^4} , \quad (2.1)$$

where, by definition,

$$B = \frac{1}{36k^2}[(\Lambda_+ - \Lambda_- - 3k^2)^2 + 12k^2\Lambda_+] , \quad (2.2)$$

$$k = 4\pi\rho , \quad (2.3)$$

and E represents the total energy of the bubble, a first integral of motion, in the form

$$E = R^3 \frac{\Lambda_- - \Lambda_+}{6} + \dot{R}^2 \frac{k}{2}[2\sigma(1 - \tfrac{1}{3}\Lambda_- R^2 + \dot{R}^2)^{1/2} - kR] , \quad (2.4)$$

where σ parametrizes the sign ambiguity related to the rate of change of the polar angle in the de Sitter conformal diagram.[12] Equation (2.1) describes a rich variety of bubble histories ranging from black-hole and wormhole solutions to bouncing solutions and to monotonically expanding or contracting solutions. The algorithm for their classification starts with the identification of the different regions in parameter space according to the sign of Λ_- and Λ_+. This is illustrated in Fig. 10 below where the parameters Λ_+ and Λ_- are expressed in units of $3k^2$. In the following discussion we take $k > 0, E > 0$ and deduce from the defining equation (2.2) that $B > 0$ when $\Lambda_+ > 0$. When $\Lambda_+ < 0$, we must distinguish two cases: (i) $\Lambda_+ < 0, \Lambda_- > 0$ then $B > 0$; (ii) $\Lambda_+ < 0, \Lambda_- < 0$, then $B < 0$ inside the region of the parameter space defined by

$$\Lambda_- - 3k^2 - (-12k^2\Lambda_-)^{1/2} < \Lambda_+ < \Lambda_- - 3k^2 + (-12k^2\Lambda_-)^{1/2} \quad (2.5)$$

which is represented by the interior of the shaded area in Fig. 10. The upper right quadrant in Fig. 10 is the parameter subspace corresponding to the action functional formulation,[10,11] while ordinary unified theories correspond to arbitrary points in parameter space according to the value of the Higgs potential.

The parameter space considered in the BGG paper consists of the positive axis $\Lambda_- > 0$ ($\Lambda_+ = 0$). It is interesting that the general formulation allows for negative values of Λ_- and Λ_+; these values correspond to an interior anti-de Sitter (AdS) phase and an exterior Schwarzschild-anti-de Sitter (SAdS) phase, respectively.

The boundary of the shaded area in Fig. 10 evidently corresponds to $B = 0$. In this case the equation of motion is still well defined but degenerates into a different equation which is not directly relevant to our discussion. Our main concern here is with the full Eq. (2.1) with $k > 0$, $E > 0$, and $B \neq 0$.

The next step in our algorithm is based on the simple observation that the equation of motion of the bubble can be interpreted as the equation of motion of a particle moving in one dimension under the influence of a potential.[10,11] This property is especially clear if we rewrite the equation of motion in dimensionless form.[12] Introducing the new variables

$$z^3 = \frac{L^2}{2E} R^3 \quad \text{and} \quad \tau' = \frac{L^2}{2k}\tau , \quad (2.6)$$

where

$$L^2 \equiv \tfrac{1}{3}[|(\Lambda_- + \Lambda_+ + 3k^2)^2 - 4\Lambda_-\Lambda_+|]^{1/2} , \quad (2.7)$$

one finds that the equation of motion takes the simple form

$$\left[\frac{dz}{d\tau'}\right]^2 = Q - V(z) , \quad (2.8)$$

where, by definition,

$$V(z) = -\left[\sigma_B z^2 + \frac{2Y}{z} + \frac{1}{z^4}\right] , \quad (2.9)$$

$$\sigma_B \equiv \mathrm{sgn} B ,$$

$$Y = \frac{1}{3}\frac{(\Lambda_+ - \Lambda_-) + 3k^2}{L^2} , \quad (2.10)$$

and

$$Q=-\frac{4k^2}{(2E)^{2/3}L^{8/3}}<0\ . \tag{2.11}$$

In addition, we introduce the auxiliary quantity

$$\tilde{Y}=\frac{1}{3}\frac{(\Lambda_+-\Lambda_-)-3k^2}{L^2} \tag{2.12}$$

and quote the simple relations

$$L^4=4k^2|B|\ , \tag{2.13}$$

$$Y^2-1=\frac{-4k^2\Lambda_-}{3L^4},\quad \tilde{Y}^2-1=-\frac{4k^2\Lambda_+}{3L^4} \tag{2.14}$$

which we have found useful in the course of our analysis. For instance, Eq. (2.13) is at the origin of the signature term in the potential $V(z)$, while the relationships (2.14) can be used to classify all possible background geometries according to the values of Y and $\tilde{Y}$. Indeed, we have three types of interior bubble geometries: (a) anti-de Sitter (AdS), for which $\Lambda_-<0$ and $Y^2>1$, (b) Minkowski (M), for which $\Lambda_-=0$ and $Y^2=1$, (c) de Sitter (dS), for which $\Lambda_->0, Y^2<1$. Each of these geometries can be matched to three kinds of exterior geometries: (α) Schwarzschild-anti-de Sitter (SAdS), for which $\Lambda_+<0$ and $\tilde{Y}^2>1$, (β) Schwarzschild (S), for which $\Lambda_+=0$ and $\tilde{Y}^2>1$, (γ) Schwarzschild-de Sitter (SdS), for which $\Lambda_+>0$ and $\tilde{Y}^2<1$. Thus, we have in principle nine possible scenarios for the bubble evolution. However, the effective control parameter is the dimensionless variable Y defined in (2.10); furthermore, the energy E appears only in the variable Q. Therefore Q, which is negative by definition, characterizes the different solutions of bubble dynamics in the dimensionless formulation.

We will discuss first the case $B>0$. The important qualitative features of the solutions can be inferred from Fig. 1 and are displayed in Fig. 2. Figure 1 represents the graph of the potential-energy function $V(z)$ for various preassigned values of Y. The potential has a single maximum whose location z_M depends on Y as

$$z_M^3=\tfrac{1}{2}[(8+Y^2)^{1/2}+Y] \tag{2.15}$$

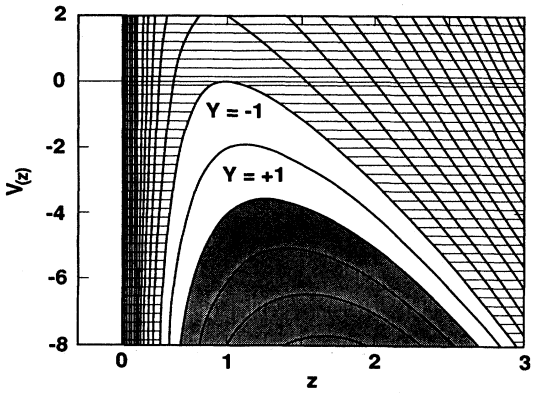

FIG. 1. A graph of the potential-energy function $V(z)$ for integer values of Y. When $|Y|<1$ the vacuum energy densities are positive.

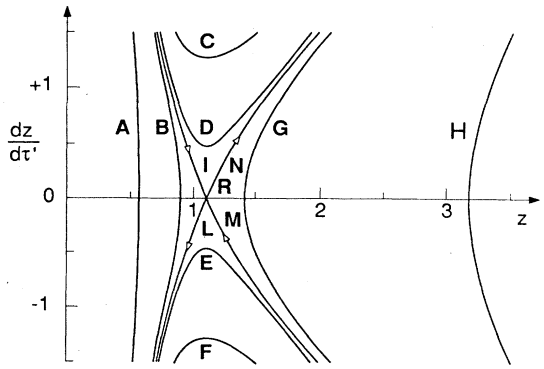

FIG. 2. The phase portrait of the vector field representing the radial equation of motion.

and the corresponding value of the potential is calculated to be

$$V_M\equiv V(z_M)=-\frac{3}{z_M^4}(z_M^6-1)\ . \tag{2.16}$$

For completeness, we also quote the expression of the *critical energy* for which $Q(E_{cr})=V(z_M)$: using Eqs. (2.11) and (2.16), this condition gives

$$E_{cr}=\frac{1}{3\sqrt{3}}\frac{4k^2}{L^4}\frac{z_M^6}{(z_M^6-1)^{3/2}}\ . \tag{2.17}$$

While Eq. (2.16) is identical to that quoted in the BGG paper,[12] the novel feature here is the "overshooting" of the potential curve over the zero threshold. In this connection we note that $0<z_M\le 1$ and $V_M\ge 0$ when $Y\le -1$ and *no bubble trajectory can exist in the region where* $V(z)>0$.

For any given value of Y, the shape of the potential curve indicates that there are at most three basic types of solutions; for later reference we shall list them as follows:[16] (i) type-I or "bounded" solutions for which there exists a maximum radius $\hat{z}$ implicitly defined by $Q=V(\hat{z})$; (ii) type-II or "bounce" solutions for which there exists a minimum radius $\tilde{z}$ defined by $Q=V(\tilde{z})$; and (iii) type-III or "monotonic" solutions for which the energy of the bubble exceeds the critical value defined by $Q(E_{cr})=V_M$.

Evidently, no monotonic solutions can exist when $Y<-1$ and the two positive roots of the equation $V(z)=0$ are

$$z_1^3=-Y-(Y^2-1)^{1/2},\quad z_2^3=-Y+(Y^2-1)^{1/2} \tag{2.18}$$

with $z_1<z_2$; of course, when $Y=-1$, $z_1=z_2=z_M=+1$. Note that in the plane of $V(z)$ vs z represented in Fig. 1, *the possible bubble trajectories correspond to straight horizontal lines with constant (negative)* Q.

An alternative representation of the three types of solutions is displayed in Fig. 2. Here the trajectories are associated with the flow of a vector field in the $(z,\dot{z})$ plane; the phase portrait of this vector field is a plot of the equation of motion itself for different values of Q at fixed Y and $V_M<0$. Trajectories A and B are of type I with

$Q < V_M$, trajectories G and H are of type II with $Q < V_M$, and trajectories C, D, E, and F are of type III with $Q > V_M$, C, and F representing the asymptotic trajectories of monotonic type corresponding to $Q = 0$. The two pairs of curves (I,L) and (M,N) are limiting trajectories with $Q = V_M$, the critical point R corresponding to z_M. These trajectories mark the transition from bounded to monotonic solutions and from bounce to monotonic solutions, respectively; trajectories I and M take an infinite proper time to reach the equilibrium point at R. Moreover, a trajectory initialized at rest at the equilibrium point, in principle remains there forever. Thus, strictly speaking, trajectories L and N can never be seen. However, the static bubble configuration of radius $z = z_M$ is unstable in the sense that an arbitrarily small perturbation will cause the bubble to either contract to zero radius along trajectory L or to expand indefinitely along trajectory N.

When $B < 0$, the shape of the potential is affected by the signature term in the defining Eq. (2.9) and one would expect a local minimum in $V(z)$ and a new class of solutions representing oscillating bubbles. However, these new solutions correspond to negative-energy bubbles and must be excluded from our classification. In order to substantiate this statement we first observe that when $B < 0$, the two roots of the equation $V(z) = 0$ are

$$z_1^3 = Y - (Y^2+1)^{1/2} < 0, \quad z_2^3 = Y + (Y^2+1)^{1/2} > 0 \tag{2.19}$$

so that the potential curve intersects the *positive* z axis at the single point z_2. Next, the two roots of the equation $V'(z) = 0$ are

$$z_M^3 = \tfrac{1}{2}[-Y \pm (Y^2-8)^{1/2}] . \tag{2.20}$$

Evidently, if $Y^2 < 8$ then $V'(z)$ never vanishes in the physical region $z > 0$ and $V(z)$ represents a function increasing monotonically from $-\infty$ to $+\infty$. Thus, for $Y^2 < 8$ one finds only type-I or bounded solutions. For $Y^2 > 8$ and $Y < 0$ the maximizing equation (2.20) gives a maximum and a minimum in the physical region $z > 0$. However, the value of the potential corresponding to the two extrema is calculated to be

$$V_M \equiv V(z_M) = \frac{3}{z_M^4}(z_M^6 + 1) > 0 . \tag{2.21}$$

The above results are summarized in Fig. 3. Thus, when $B < 0$ a local minimum of $V(z)$ exists but it lies above the z axis and corresponds to negative-energy solutions which we have excluded from our present discussion.

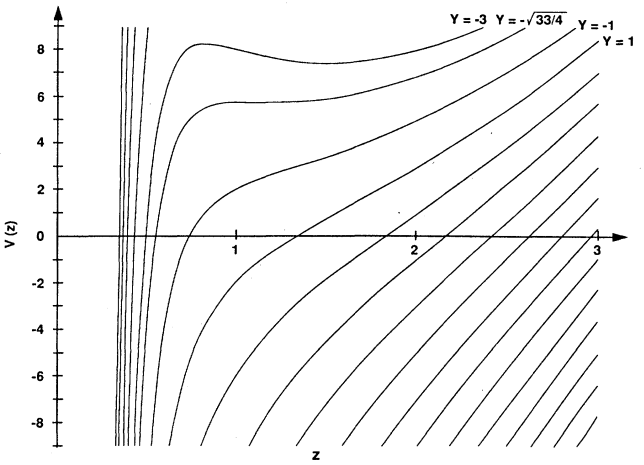

FIG. 3. A graph of the potential-energy function $V(z)$, in the case $B < 0$, for different values of Y. Notice that the local minimum of the function $V(z)$ is always above the z axis, so oscillating bubbles are classically forbidden because they would have negative mass energy.

III. THE ALGORITHM

The results of the previous section show that we can broadly classify the solutions of Eq. (2.8) according to their type, i.e., bounded, bounce, or monotonic solutions and according to the background geometry. As an example, dS-SdS-I means a bounded de Sitter bubble in a Schwarzschild–de Sitter spacetime. Actually, this information is not enough to give a full characterization of the bubble dynamics. For instance, at this stage one cannot distinguish between solutions evolving into black holes or wormholes. An extra variable is required to describe the evolution of the bubble in relation to the cosmological horizons.

Accordingly, we define a new "landmark" in our classification as the value of the coordinate z where the curve representing the de Sitter (or Schwarzschild–de Sitter) horizon is tangent to the potential curve $V(z)$. Following the format used by Blau, Guendelman, and Guth,[12] first we have to determine the *horizon curves* in terms of our dimensionless variables defined in Eqs. (2.6)–(2.12). The de Sitter spacetime exhibits a cosmological event horizon only if $\Lambda_- > 0$, which implies $|Y| < 1$. In terms of the z coordinate the de Sitter horizon radius takes the form $z_{dS} = (L^2/2E)^{1/3}(3/\Lambda_-)^{1/2}$. Then, taking into account the first of Eqs. (2.14), it is easy to derive the de Sitter horizon equation

$$Q = (Y^2-1)z_{dS}^2 \equiv V(z_{dS}) + \frac{1}{z_{dS}^4}(1 + Yz_{dS}^3)^2 . \tag{3.1}$$

To find the analogous equation for the Schwarzschild–de Sitter horizon is slightly more involved since, in principle, one could find two, one, or no horizons[18] according to the value of the ratio $\Lambda_+/9E^2$. The horizons are defined as the roots of the algebraic equation

$$1 - \frac{2E}{R_{SdS}} - \frac{\Lambda_+}{3} R_{SdS}^2 = 0 . \tag{3.2}$$

Since

$$\tilde{Y}^2 - 1 = -4k^2 \frac{\Lambda_+}{3L^4} , \tag{3.3}$$

and

$$Y - \tilde{Y} = \frac{2k^2}{L^2} , \tag{3.4}$$

Eq. (3.2) can be written in dimensionless form as

$$Q=(\tilde{Y}^2-1)z_{\rm SdS}^2-2(Y-\tilde{Y})\frac{1}{z_{\rm SdS}}$$
$$\equiv V(z_{\rm SdS})+\frac{1}{z_{\rm SdS}^4}(1+\tilde{Y}z_{\rm SdS}^3)^2 . \quad (3.5)$$

The advantage of this formulation, which is an extension of the BGG analysis[12] for $-1\le Y\le 1$ with $\Lambda_+=0$, stems from our earlier observation that in the $V-z$ plane of Fig. 1 the bubble trajectories are represented by straight horizontal lines corresponding to a fixed value of Q. Evidently, in the same V-z plane and for a *preassigned* value of the energy, the corresponding values of the horizon *radii* are determined by the intersections, if any, between the bubble trajectory with fixed Q and the horizon curve (3.5). The analytical basis of our graphical method is as follows: for $\Lambda_+>0$, or $\tilde{Y}^2<1$ there is a single maximum in the horizon curve at

$$z_m=\left[\frac{3L^2}{2\Lambda_+}\right]^{1/3}, \quad (3.6)$$

where Q takes on the value

$$Q(z_m)=-\frac{4k^2}{L^{8/3}}\left[\frac{3}{2}\right]^{2/3}(\Lambda_+)^{1/3} \quad (3.7)$$

or, in terms of E, via Eq. (2.11),

$$\frac{1}{3E}=\sqrt{\Lambda_+} \quad (3.8)$$

which is just the condition for having a single horizon in the SdS metric.[17] For $3E<\sqrt{\Lambda_+}$ there are two intersections in the region $z>0$ corresponding to two physical horizon; they coalesce when Eq. (3.8) holds, and no horizon exists in the physical region if $3E>\sqrt{\Lambda_+}$.

On the other hand, for $\Lambda_+<0$, or $\tilde{Y}^2>1$, there is a single horizon at

$$r_0=\left[-\frac{3E}{\Lambda_+}+\left[\frac{\sqrt{9}E^2}{\Lambda_+^2}-\frac{1}{\Lambda_+^3}\right]^{1/2}\right]^{1/3}$$
$$+\left[-\frac{3E}{\Lambda_+}-\left[\frac{\sqrt{9}E^2}{\Lambda_+^2}-\frac{1}{\Lambda_+^3}\right]^{1/2}\right]^{1/3},$$

and in fact the horizon curve is monotonically increasing for $z>0$; there is no stationary point in the physical region. Hence, for any assigned value of E there is a single intersection with the curve (3.5) providing the correct value of the horizon coordinate.

So, all the complexity pertaining to the global structure of the SdS spacetime is encoded into the simple Eq. (3.5).

Now we can determine the points where the horizons are tangent to $V(z)$. In the de Sitter case the contact point is

$$z_{\rm dS}^3=-\frac{1}{Y}, \quad -1\le Y<0 \quad (3.9)$$

while the Schwarzschild–de Sitter horizon is tangent to $V(z)$ at

$$z_{\rm SdS}^3=-\frac{1}{\tilde{Y}}, \quad -1\le\tilde{Y}<0 . \quad (3.10)$$

The corresponding values of the potential $V(z)$ are

$$V_{\rm dS}\equiv V(z_{\rm dS})=\frac{Y^2-1}{Y^{2/3}} \quad (3.11)$$

and

$$V_{\rm SdS}\equiv V(z_{\rm SdS})=-\frac{\tilde{Y}^2-2Y\tilde{Y}+1}{\tilde{Y}^{2/3}} . \quad (3.12)$$

In the above interpretation, the bounded (bounce) trajectory of a bubble for which the maximum (minimum) attainable radius is precisely $z_{\rm SdS}$ ($z_{\rm dS}$) acquires a special status: for this to happen, the energy of the bubble must be exactly tuned so that either $Q=V(z_{\rm SdS})$ or $Q=V(z_{\rm dS})$. These conditions give

$$E_{\rm SdS}=-\frac{4k^3}{L^4}\frac{\tilde{Y}}{(\tilde{Y}^2-2Y\tilde{Y}+1)^{3/2}} \quad (3.13)$$

or

$$E_{\rm dS}=-\frac{4k^3}{L^4}\frac{Y}{(1-Y^2)^{3/2}} . \quad (3.14)$$

Having identified the new landmarks (3.9) and (3.10), the above discussion requires some qualifications. Note first that $z_{\rm dS}$ and $z_{\rm SdS}$ are defined for $Y<0$ and $\tilde{Y}<0$. In addition, we note that when $Y\le -1$ then the value $V(z_{\rm dS})$ of the potential $V(z)$ at $z_{\rm dS}$ is ≥ 0. This property reflects the fact that Eq. (3.1) has no physical meaning for $Y\le -1$ since $\Lambda_-<0$ and the interior "horizon" is undefined for anti-de Sitter space. When $Y\le -1$, the mathematical curve (3.1) is still tangent to the potential curve but the tangent point is in the unphysical region where $V(z)\ge 0$.

Another property of $z_{\rm SdS}$ and $z_{\rm dS}$ is based on the proven equivalence between the equation of motion (2.1) and Israel's equation in the form

$$\beta_{\rm dS}-\beta_{\rm SdS}=kR , \quad (3.15)$$

where

$$\beta_{\rm dS}=\sigma\left[1-\frac{\Lambda_-}{3}R^2+\dot{R}^2\right]^{1/2} \quad (3.16)$$

and

$$\beta_{\rm SdS}=\sigma\left[1-\frac{\Lambda_+}{3}R^2-\frac{2E}{R}+\dot{R}^2\right]^{1/2} . \quad (3.17)$$

Inspection of the form of $\beta_{\rm dS}$ and $\beta_{\rm SdS}$ indicates that they vanish at the point where the horizon curves are tangent to the potential-energy curve $V(z)$. Indeed, in terms of our dimensionless variables Y, z, and Q, we find

$$\beta_{\rm dS}=|Q|^{-1/2}\frac{1+Yz^3}{z^2} \quad (3.18)$$

and

$$\beta_{\rm SdS}=|Q|^{-1/2}\frac{1+\tilde{Y}z^3}{z^2} . \quad (3.19)$$

Since $\beta_{\rm SdS}$ and $\beta_{\rm dS}$ are monotonic functions of z, the switch in sign occurs at

$$z_{\rm SdS}^3=-\frac{1}{\tilde{Y}} \quad (\text{for } \beta_{\rm SdS})$$

and (3.20)

$$z_{\rm dS}^3 = -\frac{1}{Y} \quad (\text{for } \beta_{\rm dS}) .$$

It is understood that Eq. (3.20) holds under the same assumptions leading to (3.9) and (3.10).

The physical role of the new landmarks can be better understood with reference to a specific example. Figure 4 describes de Sitter bubbles in a Schwarzschild–de Sitter background, with $Y=-0.2182$, $\tilde{Y}=-0.6547$. Some typical trajectories are labeled according to the notation[12] of BGG and the corresponding conformal diagrams are drawn according to the rules discussed by Walker.[18]

(A) This is a small-mass type-I solution. All along the trajectory both $\beta_{\rm SdS}$ and $\beta_{\rm dS}$ are positive, so that the polar angle in SdS spacetime is always increasing while it decreases in the interior of dS space. Such a behavior is described by the Penrose diagrams in Fig. 5. These configurations are generalizations of the black-hole solutions of Refs. 7 and 8.

(C) This is a type-II bounce solution. The minimum radius is larger than $z_{\rm dS}$ and $z_{\rm SdS}$. The bubble crosses both the dS and SdS horizons but evolves always outside the black-hole SdS horizon. Both $\beta_{\rm SdS}$ and $\beta_{\rm dS}$ are negative indicating that the SdS polar angle is decreasing while the dS polar angle is increasing. See Fig. 6.

(D) This is again a type-II solution, but now the minimum radius is smaller than $z_{\rm dS}$ and still larger than $z_{\rm SdS}$. So, $\beta_{\rm dS}$ changes its sign along this trajectory before the dS horizon is crossed. For the external observers the Penrose diagram is the same as in case (C), while for the internal observers the bubble crosses sector III of the dS Penrose diagram rather than sector I. See Fig. 7.

The following cases do not fit into the BGG classification.

(F) This is a type-III monotonic solution. It differs from the BGG E bubble because $\beta_{\rm SdS}$ changes sign after the trajectory has crossed the cosmological SdS horizon, so that the bubble goes through region I instead of region III of the SdS Penrose diagram. A static observer in I is then doomed to crash against the expanding bubble wall. See Fig. 8. The only way out is to fall through the cosmological event horizon before the bubble arrival.

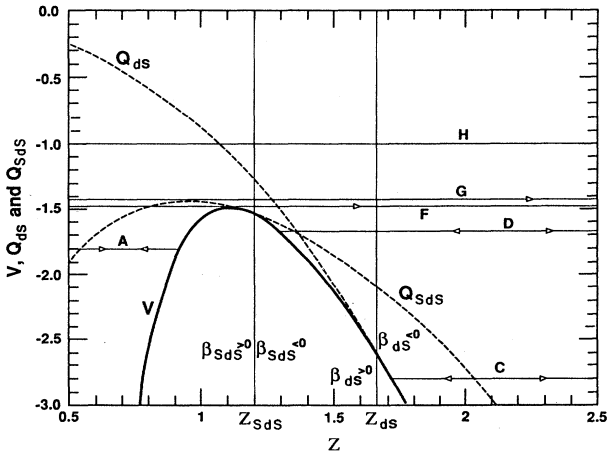

FIG. 4. An example of the numerical-graphical method to determine the admissible solutions for a given point $(\Lambda_+/3k^2=3, \Lambda_-/3k^2=5)$ in the parameter space of Fig. 10. The corresponding values of Y and $\tilde{Y}$ are $Y=-0.2182$, $\tilde{Y}=-0.6547$.

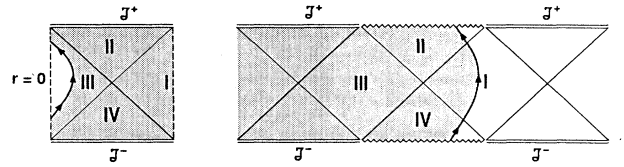

FIG. 5. Penrose diagram for a type-I bounded solution. (Here and in the following the dashed areas have to be removed and the two diagrams matched along the trajectory.) The bubble expands up to the maximum radius $\hat{z}$, and then collapses into a SdS black hole.

(G) This is a limiting type-III solution, in the sense that the mass E^* of the bubble is fine-tuned to satisfy $Q(E^*)=Q(z_m)$. In this case the two horizons of the SdS metric degenerate into a single null surface $\tilde{r}=1/\sqrt{\Lambda_+}$. The corresponding Penrose diagram is in Fig. 9. Everything goes like in (F).

(H) This is a type-III solution with $Q>Q(E^*)$. The exterior geometry has no horizons. The corresponding conformal diagram consists of a horizontal infinite strip such as the right-hand side of Fig. 9 with the horizon lines excised, bounded from below by the $r=0$ singularity and from above by "script" I^+. The actual diagram, which we do not reproduce here, can be found in Fig. 3(c) of the first paper quoted in Ref. 6. As far as the internal observer is concerned the bubble evolution is the same as in (G).

The quoted examples are far from exhausting all possible physical configurations of the system. A detailed analysis of the other cases is postponed to a future paper. Rather, the central question to be addressed now is how to determine the admissible solutions for a given set of values of the parameters $\Lambda_+/3k^2$ and $\Lambda_-/3k^2$. This brings us to Fig. 10 which is a map of the parameter space with all the landmarks which are relevant to our discussion. The shaded area and its boundary were discussed at the beginning of the paper; we simply add here that, in order to give a meaning to the solutions with $L^2=0$, one must refer to the equation of motion in its original form (2.1). The meaning of the other landmarks on the map is as follows: the parallel lines $\overline{QX}$ and $\overline{RW}$ are defined by the equations $Y=0$ and $\tilde{Y}=0$, respectively; $Q(-1,0)$ and $R(0,-1)$ are branching points where Y and $\tilde{Y}$ are, respectively, undefined; on the vertical axis,

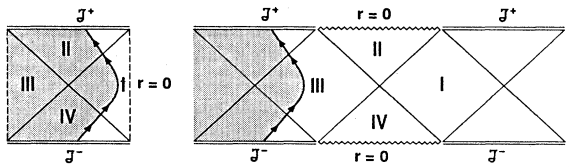

FIG. 6. Penrose diagram for a type-II bounce solution.

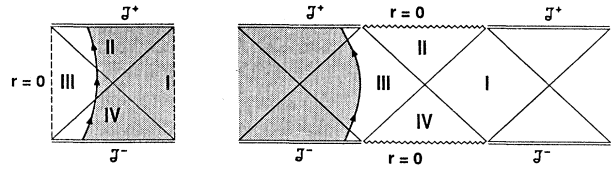

FIG. 7. This is again the Penrose diagram for a bouncing solution, but now β_{dS} changes sign before the dS horizon curve is reached. The trajectory crosses region III of the dS manifold rather than region I as in the previous case.

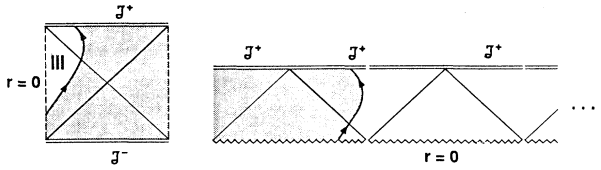

FIG. 9. This is the extreme SdS case exhibiting a single degenerate horizon. The bubble is again described by a monotonic type-III solution.

$\tilde{Y}=+1$ below point R and $\tilde{Y}=-1$ above R; on the horizontal axis, $Y=+1$ to the right of Q; to the left of Q, $Y=-1$ and therefore $z_1=z_M=z_{dS}=z_2=1$, $V(z_1)=V(z_M)=V(z_{dS})=V(z_2)=0$, the interior de Sitter horizon is undefined, and the SdS horizon is tangent to $V(z)$ at $z_{SdS}=L^2/(L^2+k^2)<1$. Thus, when $Y=-1$, $z_{SdS}<z_M=z_{dS}$ and

$$V(z_{SdS})=-\frac{(\tilde{Y}+1)^2}{\tilde{Y}^{2/3}}<0\ . \tag{3.21}$$

The set of points where $V_{SdS}=V(z_{SdS})=0$ consists of the line $\overline{AB}$ in the region where $Y<-1$ and

$$\tilde{Y}^2-2Y\tilde{Y}+1=0 \tag{3.22}$$

or

$$\frac{\Lambda_-}{3k^2}=-1, \quad \text{so that } z_{SdS}=z_1\ . \tag{3.23}$$

As noted earlier, no monotonic solutions can exist for $Y<-1$. Finally, the set of points in parameter space where $z_{SdS}=z_M$ consists of the line $\overline{RY}$ where

$$\frac{\Lambda_-}{3k^2}=3\frac{\Lambda_+}{3k^2}-1\ . \tag{3.24}$$

Thus, to the right of the line $\overline{RY}$, $z_M<z_{sD}$; the value of Y can be positive or negative but >-1 so that $V(z_{SdS})<V(z_M)<0$ and monotonic solutions can exist. The de Sitter horizon and the SdS horizon are both well defined in this region.

The algorithm to determine the set of admissible solutions proceeds along the following steps: (1) a point $(\Lambda_+/3k^2, \Lambda_-/3k^2)$ is assigned in any given region of parameter space; (2) $L^2, Y, \tilde{Y}$ are calculated using Eqs. (2.7), (2.10), and (2.12); (3) z_M, z_{dS} and z_{SdS} are calculated using Eqs. (2.15), (3.9), and (3.10); (4) V_M, V_{dS}, and V_{SdS} are calculated using Eqs. (2.16), (3.11), and (3.12); (5) the horizon curves and the potential-energy curve $V(z)$ are plotted using Eqs. (3.1), (3.5), and (2.9).

The above procedure automatically selects a possible solution for any allowed value of the bubble energy E or Q. Figure 4 shows an explicit application of the algorithm (steps 1–5). Once a value of Q is selected, the location of the trajectories relative to the horizon curves and $V(z)$ gives all the necessary information to reconstruct the detailed evolution of the bubble.

In conclusion, the algorithm proposed in this paper shows that the history of a spherical bubble in a vacuum can be analyzed algebraically in terms of the potential $V(z)$ and the horizon curves. There are many applications of the various families of solutions. For instance, the study of localized inflation in the early Universe discussed in the BGG paper,[12] focuses mostly on monotonically expanding solutions; in the general formulation we find that these solutions are not always permitted and we have specified the domain in parameter space where such solutions are excluded. In connection with the confinement mechanism in the bag model,[3,4] where the

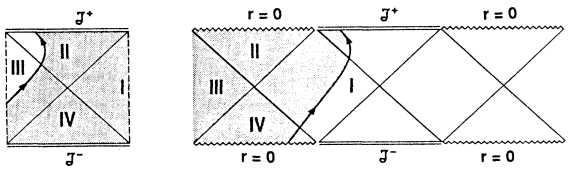

FIG. 8. Penrose diagram for a type-III unbounded trajectory. The world line of any static observer in region I of the SdS manifold is crossed by the bubble trajectory.

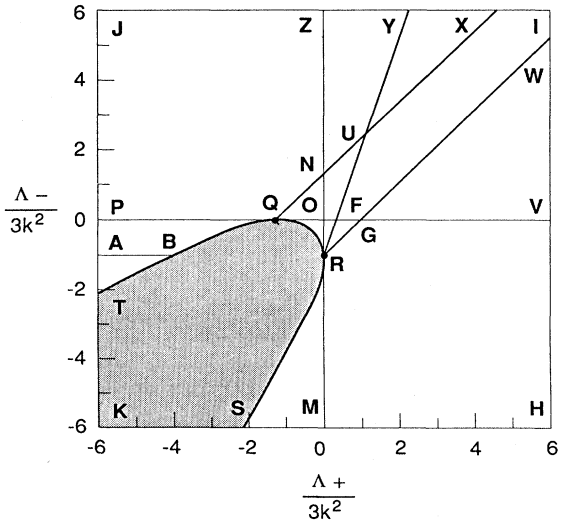

FIG. 10. The complete map of parameter space with all the "landmarks" which are necessary in the classification of the possible solutions. The interior of the shaded region corresponds to $B<0$; on the boundary of this region $L^2=0$ and the values of Y and $\tilde{Y}$ are undefined. Any other region on the map is characterized by a definite value of Y and $\tilde{Y}$.

bag constant plays the role of a cosmological constant in the hadronic vacuum, the interest is mostly on bounded, or "black-hole" solutions.

Finally, it would appear that "baby-universe" solutions, once included in the Euclidean path integral of quantum gravity, may bridge the gap between microphysics and the large-scale structure of the Universe, thus offering a possible solution to the long-standing problem of the zero value of the cosmological constant.[15] In this connection, we note that the action functional formulation[11] of bubble dynamics is the natural framework to extend our results to Euclidean space; this extension is necessary if one is interested, for instance, in the classification of the bubble Euclidean trajectories in connection with tunneling processes in false vacuum decay[5] or in connection with the problem of the cosmological constant. These interesting problems will have to be the subject of a separate investigaton.

ACKNOWLEDGMENTS

One of the authors (A.A.) wishes to thank the Associated Western Universities, Incorporated, for financial support while at the Stanford Linear Accelerator Center. Two of us (A.A. and M.P.) would also like to thank the President, the Dean of the College of Science, and the Physics Chair at California State Polytechnic University, Pomona, for their support in the form of reassigned time, a travel grant, and a research grant under the California State University Research, Scholarship, and Creative Activity Program. Finally, A.A. would like to thank the staff, the faculty, and the students in the Theory Group at SLAC for their assistance and for the hospitality extended to him. Special thanks go to Kent Hornbostel for plotting some of the graphs. This work was supported by the Department of Energy, Contract No. DE-AC03-76SF00515.

[1]P. A. M. Dirac, Proc. R. Soc. London **A268**, 57 (1962); P. A. Collins and R. W. Tucker, Nucl. Phys. **B112**, 150 (1976).

[2]A. Aurilia and D. Christodoulou, J. Math. Phys. **20**, 1446 (1989); **20**, 1692 (1979).

[3]A. Aurilia and D. Christodoulou, Phys. Lett. **78B**, 589 (1978).

[4]A. Aurilia, Phys. Lett. **81B**, 203 (1979).

[5]S. Coleman, Phys. Rev. D **15**, 2929 (1977); S. Coleman and F. De Luccia, *ibid.* **21**, 3305 (1980); S. Parke, Phys. Lett. **121B**, 313 (1983); W. A. Hiscock, Phys. Rev. D **35**, 1161 (1987).

[6]K. Maeda, H. Sato, M. Sasaki, and H. Kodama, Phys. Lett. **108B**, 98 (1982); K. Maeda, M. Sasaki, and H. Sato, Prog. Theor. Phys. **69**, 89 (1983); K. Maeda and H. Sato, *ibid.* **70**, 772 (1983); **70**, 1276 (1983).

[7]V. A. Berezin, V. A. Kuzmin, and I. I. Tkachev, Phys. Lett. **120B**, 91 (1983).

[8]J. Ipser and P. Sikivie, Phys. Rev. D **30**, 712 (1984); J. Ipser, *ibid.* **30**, 2452 (1984); Ya. B. Zeldovich and M. Yu. Khlopov, Phys. Lett. **79B**, 239 (1978).

[9]K. Lake and R. Wevrick, Can. J. Phys. **64**, 165 (1986).

[10]A. Aurilia, G. Denardo, F. Legovini, and E. Spallucci, Phys. Lett. **147B**, 258 (1984); Nucl. Phys. **B252**, 523 (1985).

[11]A. Aurilia, R. S. Kissack, R. Mann, and E. Spallucci, Phys. Rev. D **35**, 2961 (1987).

[12]S. K. Blau, E. I. Guendelman, and A. H. Guth, Phys. Rev. D **35**, 1747 (1987).

[13]W. Israel, Nuovo Cimento **44B**, 1 (1966); **48B**, 463 (1967); see also J. E. Chase, *ibid.* **67B**, 136 (1970); S. O'Brien and J. L. Synge, Commun. Dublin Inst. Adv. Stud. **9A**, 1 (1952).

[14]The bubble equation of motion reported in Ref. 10 has an incorrect sign. The equation of motion was correctly written in Ref. 11 and is reported here as Eq. (2.1).

[15]S. Coleman, Nucl. Phys. **B310**, 643 (1988); T. Banks, *ibid.* **B309**, 493 (1988).

[16]For the corresponding classification in the Minkowski vacuum, see Ref. 3.

[17]K. Lake and R. C. Roeder, Phys. Rev. D **15**, 3513 (1977).

[18]M. Walker, J. Math. Phys. **11**, 2280 (1970).

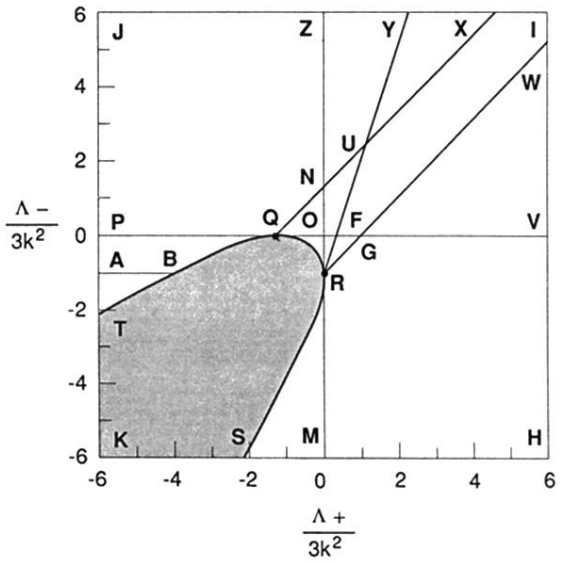

FIG. 10. The complete map of parameter space with all the "landmarks" which are necessary in the classification of the possible solutions. The interior of the shaded region corresponds to $B<0$; on the boundary of this region $L^2=0$ and the values of Y and $\tilde{Y}$ are undefined. Any other region on the map is characterized by a definite value of Y and $\tilde{Y}$.

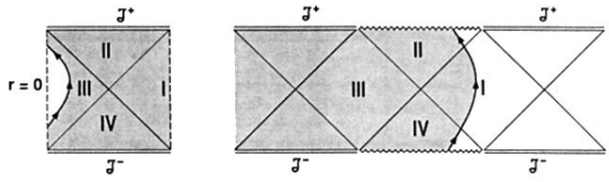

FIG. 5. Penrose diagram for a type-I bounded solution. (Here and in the following the dashed areas have to be removed and the two diagrams matched along the trajectory.) The bubble expands up to the maximum radius $\hat{z}$, and then collapses into a SdS black hole.

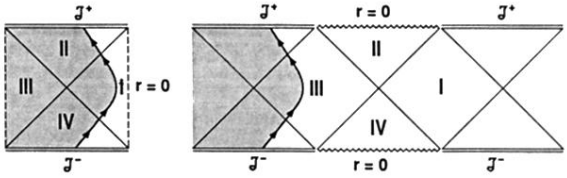

FIG. 6. Penrose diagram for a type-II bounce solution.

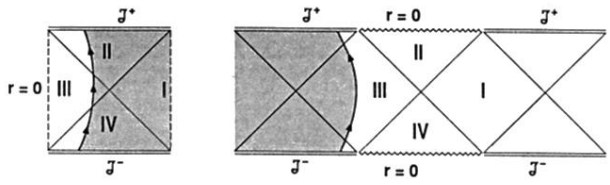

FIG. 7. This is again the Penrose diagram for a bouncing solution, but now $\beta_{\rm dS}$ changes sign before the dS horizon curve is reached. The trajectory crosses region III of the dS manifold rather than region I as in the previous case.

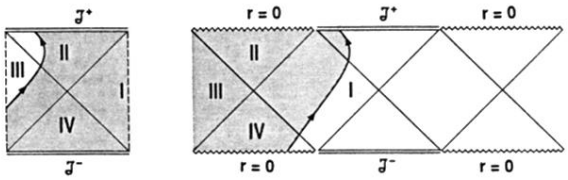

FIG. 8. Penrose diagram for a type-III unbounded trajectory. The world line of any static observer in region I of the SdS manifold is crossed by the bubble trajectory.

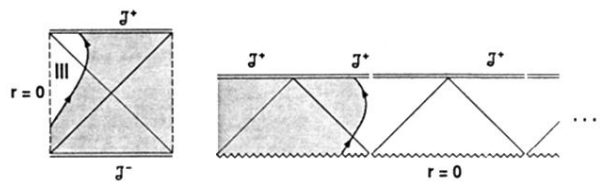

FIG. 9. This is the extreme SdS case exhibiting a single degenerate horizon. The bubble is again described by a monotonic type-III solution.